



Article

# Facile Fabrication of CeO<sub>2</sub>/Electrochemically Reduced Graphene Oxide Nanocomposites for Vanillin Detection in Commercial Food Products

Xue Nie <sup>1,2</sup>, Rui Zhang <sup>1</sup>, Zheng Tang <sup>1</sup>, Haiyan Wang <sup>1</sup>, Peihong Deng <sup>2</sup> and Yougen Tang <sup>1,\*</sup>

<sup>1</sup> College of Chemistry and Chemical Engineering, Central South University, Changsha 410083, China; hynuniexue@126.com (X.N.); csuzr606@csu.edu.cn (R.Z.); tangzhenggz@csu.edu.cn (Z.T.); wanghy419@126.com (H.W.)

<sup>2</sup> Key Laboratory of Functional Metal-Organic Compounds of Hunan Province, Key Laboratory of Functional Organometallic Materials of Hunan Provincial Universities, College of Chemistry and Material Science, Hengyang Normal University, Hengyang 421008, China; dph1975@163.com

\* Correspondence: ygtang@csu.edu.cn; Tel.: +86-07318830886; Fax: +86-07318879616

Received: 4 June 2020; Accepted: 9 July 2020; Published: 11 July 2020



**Abstract:** In this paper, CeO<sub>2</sub> nanoparticles were synthesized by the solvothermal method and dispersed uniformly in graphene oxide (GO) aqueous solution by ultrasonication. The homogeneous CeO<sub>2</sub>-GO dispersion was coated on the surface of a glassy carbon electrode (GCE), and the CeO<sub>2</sub>/electrochemically reduced graphene oxide modified electrode (CeO<sub>2</sub>/ERGO/GCE) was obtained by potentiostatic reduction. The results of X-ray diffraction (XRD), energy dispersive X-ray spectroscopy (EDS), scanning electron microscopy (SEM), and transmission electron microscopy (TEM) showed that CeO<sub>2</sub> nanocrystals were uniformly coated by gossamer like ERGO nanosheets. The electrochemical behavior of vanillin on the CeO<sub>2</sub>/ERGO/GCE was studied by cyclic voltammetry (CV). It was found that the CeO<sub>2</sub>/ERGO/GCE has high electrocatalytic activity and good electrochemical performance for vanillin oxidation. Using the second derivative linear sweep voltammetry (SDLSV), the CeO<sub>2</sub>/ERGO/GCE provides a wide range of 0.04–20 μM and 20 μM–100 μM for vanillin detection, and the detection limit is estimated to be 0.01 μM after 120 s accumulation. This method has been successfully applied to the vanillin detection in some commercial foods.

**Keywords:** CeO<sub>2</sub> nanoparticles; vanillin; reduced graphene oxide; nanocomposites; voltammetric determination

## 1. Introduction

The problem of food safety has caused public concern all over the world. Unsafe food can lead to many acute and lifelong diseases, from diarrhea to various cancers [1]. Vanillin (4-hydroxy-3-methoxybenzaldehyde), a food additive, is widely used to contribute to the fragrance of various foods, such as ice-cream, cookies, pudding, beverages, custard, and chocolate [2]. However, the production cost of natural vanillin from vanilla pods is very high. Low-cost materials, such as eugenol, 2-methoxyphenol, and lignin, can also be used to synthesize vanillin. Although the synthetic version is cheaper and widely produced, it can lead to headaches, nausea, vomiting, and may affect the functions of the kidneys and liver when large quantities of vanillin are ingested. Therefore, for the sake of human health, the content of vanillin in food should be strictly controlled.

In order to determine vanillin sensitively and effectively, gas chromatography [3], high performance liquid chromatography [4], thin layer chromatography [5], ultraviolet visible spectrophotometry [6], chemiluminometry [7], and capillary electrophoresis [8] were introduced. However, most of these methods need large and expensive instruments, and the operation is complex and time-consuming. The electrochemical method has been one of the research hotspots due to its advantages of easy

operation, excellent sensitivity, and low cost. Although vanillin molecules are electrooxidable, the results of direct determination of vanillin with bare electrode are not satisfactory. The main reason is that the fouling and regeneration of electrode surface [2]. In recent years, new electrochemical sensing methods using chemically modified electrodes (CMEs) for vanillin detection have been investigated [9–18]. For example, Shang et al. developed a vanillin electrochemical sensor based on AuPd-graphene hybrid. They found that the sensor exhibited high electrocatalytic activity towards vanillin oxidation and the electrochemical response was greatly increased [9]. Sivakumar et al. prepared a glassy carbon electrode (GCE) modified with a CoS nanorods–Nafion composite which can be applied for vanillin detection in food samples [10]. Mei et al. reported an electrospun molybdenum disulfide-carbon nanofiber (MoS<sub>2</sub>-CNF) for vanillin detection. In the concentration range of 0.3–135 μM, the peak current shows a good linear response, and the detection limit is 0.15 μM [11]. However, the performance of some modified electrodes is still not ideal due to the poor electrocatalytic activity of the modified materials. Therefore, it is very important to prepare novel modified electrodes for the rapid and effective detection of vanillin.

Graphene (GR) is a kind of planar monolayer structure composed of sp<sup>2</sup>-bonded carbon atoms. With its high specific surface area, unique mechanical and electronic properties, GR has attracted tremendous attention [19]. The properties of GR can be adjusted by surface modification. The organic functionalization and inorganic nanoparticles attachments on the surface of GR significantly changed the physical and chemical properties of GR and greatly expanded its application field [20–24]. Recently, lots of researches have been carried out to modify the surface of GR with MnO<sub>2</sub> [25,26], SnO<sub>2</sub> [27], Fe<sub>3</sub>O<sub>4</sub> [28,29], Co<sub>3</sub>O<sub>4</sub> [30], Cu<sub>2</sub>O [31–33], NiO [34], TiO<sub>2</sub> [35], and other metal oxide nanoparticles, and to find their applications in electrode modification. CeO<sub>2</sub> nanoparticles have the advantages of low cost, excellent electrochemical redox characteristic, and environmental friendliness, and are explored as an excellent electrode modifier material [36]. For example, Adarakatti et al. fabricated a GCE modified with mesoporous CeO<sub>2</sub> nanoparticles and used for the determination of Cu (II) and Hg (II) [37]. Cai and coworkers fabricated an electrochemical immunosensor based on CeO<sub>2</sub>/chitosan nanocomposite for the determination of sulfamethoxazole in foods [38]. Dong et al. synthesized a novel multi-walled carbon nanotubes (MWCNT)–CeO<sub>2</sub>–Au nanocomposite and realized the successful detection of methyl parathion [39]. However, CeO<sub>2</sub> nanoparticles as an electrode material have some problems, such as easy agglomeration and poor conductivity, which seriously affect its performance in practical applications. Anchoring CeO<sub>2</sub> on the GR nanosheets with large specific surface area and high conductivity can effectively solve these problems. Some researchers have made great efforts in the preparation of CeO<sub>2</sub>/GR nanocomposites for supercapacitors [40,41]. However, as far as we know, using CeO<sub>2</sub>/GR nanocomposites for electrochemical sensing has not been reported in any literature. In previous reports, most of the methods for CeO<sub>2</sub>/GR preparation are multi-step, involving dangerous or toxic reducing agents, which are prone to environmental and health risks. Furthermore, due to the poor dispersibility of GR nanosheets in the solvents, GR nanosheets tend to agglomerate together by van der Waals interaction and strong π–π stacking, which limit the application in the electrode modification.

In this paper, CeO<sub>2</sub>/graphene oxide (GO) nanocomposites were prepared by the ultrasonic mixing of GO solution and CeO<sub>2</sub> nanoparticles, and the CeO<sub>2</sub>/ERGO/GCE was obtained by coating the suspension by drop-coating method and further treated by potentiostatic reduction at –1.2 V for 120 s. This method offers several advantages over other techniques for the preparation of CeO<sub>2</sub>/GR nanocomposite, including being green, efficient, inexpensive, and rapid. The electrochemical behavior of vanillin was investigated on the CeO<sub>2</sub>/ERGO/GCE for the first time. Due to the advantages of each component material and their synergistic effect, the CeO<sub>2</sub>-ERGO nanocomposites significantly improved the performance of the sensor. In addition, the CeO<sub>2</sub>/ERGO/GCE exhibited good reproducibility, high accuracy, and strong anti-interference ability for vanillin detection. More importantly, because the electrode was modified in one step, the electrode fabrication is very convenient and fast. The developed sensor has a wide application prospect in the determination of vanillin in food.

## 2. Experimental

### 2.1. Chemicals

Cerium nitrate hexahydrate was purchased from Chengdu Aikeda Chemical Reagent Co., Ltd. (Chengdu, China). Vanillin, graphite powder, potassium permanganate, sodium nitrate, ethylene glycol, hydrogen peroxide solution (30 wt %), ammonia solution (25 wt %), and hydrazine solution (80 wt %) were obtained from Sinopharm Group Chemical Reagent Co., Ltd. (Shanghai, China). The accurately weighed vanillin was dissolved in a proper amount of ethanol, diluted with water to obtain a 1.0 mM stock solution. Other chemicals used in the experiment are of analytical reagent grade. The water used is ultrapure water.

### 2.2. Apparatus

Electrochemical experiments (cyclic voltammetry and second-order derivative linear sweep voltammetry) were carried out on a chi660e electrochemical workstation (Shanghai Chenhua Instrument Co., Ltd., Shanghai, China) and JP-303E polarographic analyzer (Chengdu Instrument Co., Ltd., Chengdu, China) respectively. A three electrode system was used, i.e., modified GCE with diameter of 3 mm was used as working electrode, and a saturated calomel electrode (SCE) and platinum wire electrode were used as reference electrode and auxiliary electrode respectively. The scanning electron microscope (SEM) images were obtained using a scanning electron microscope (EVO10, ZEISS, Jena, Germany). Transmission electron microscope (TEM) images and energy dispersive X-ray spectroscopy (EDS) were obtained by a transmission electron microscope (JEOL JEM-2100, Tokyo, Japan). The X-ray diffraction data (XRD) were collected on a powder X-ray diffractometer (Rigaku, Tokyo, Japan) (Cu K $\alpha$  radiation  $\lambda = 0.154056$  nm). All measurements were performed at room temperature.

### 2.3. Synthesis of CeO<sub>2</sub> Nanoparticles

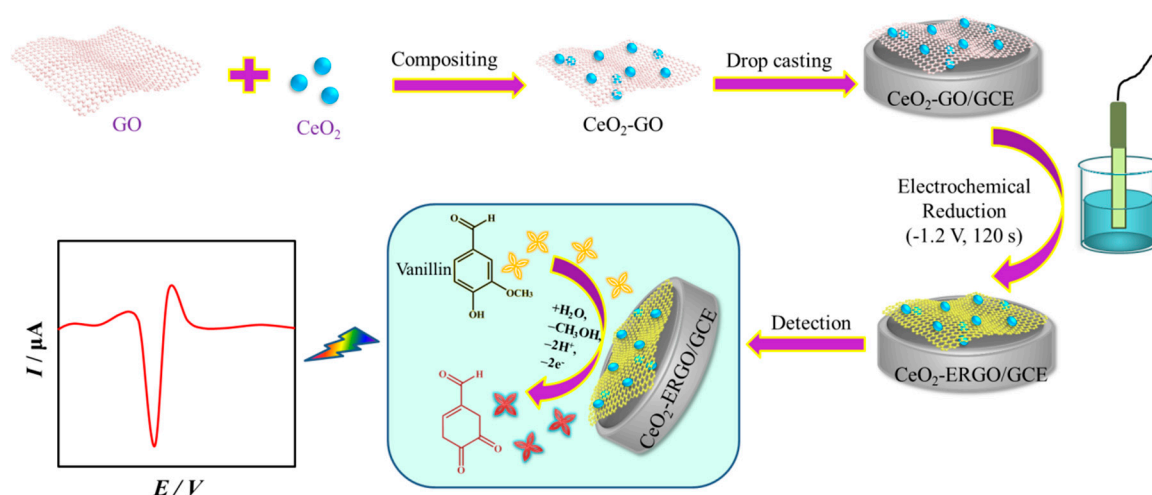
CeO<sub>2</sub> nanoparticles were synthesized via a hydrothermal method. In brief, 1 mL of 0.5 M cerium nitrate aqueous solution was added to 30 mL of ethylene glycol, followed by the addition of 1 mL of ultrapure water, the mixed solution was stirred for 30 min at room temperature and transferred to a 50 mL autoclave for solvothermal reaction at 140 °C for 18 h. After the reaction, the mixture was cooled down to room temperature. The product was centrifuged, washed with water and ethanol, and dried in an oven at 50 °C.

### 2.4. Preparation of GO and CeO<sub>2</sub>-GO Composite

Graphene oxide (GO) was prepared using a modified Hummers method, which involves the steps of graphite oxidation and subsequent exfoliation [42]. A homogeneous CeO<sub>2</sub>-GO dispersion was obtained by mixing 1.0 mg of the CeO<sub>2</sub> nanoparticles and 1.0 mL GO solution (1 mg mL<sup>-1</sup>) directly by ultrasonication for 20 min.

### 2.5. Fabrication of Modified Electrodes

Before modification, a GCE was polished on a polishing cloth with 0.3  $\mu$ m alumina powder, and then ultrasonic treatment was carried out in ethanol and ultrapure water successively. A treated GCE was modified with 5.0  $\mu$ L of CeO<sub>2</sub>-GO dispersion and the solvent on the electrode surface was evaporated under an infrared lamp. Then the electrode was put into a 0.1 M phosphate buffer (pH 6.5) and reduced at the constant potential of  $-1.2$  V for 120 s to obtain the CeO<sub>2</sub>/ERGO/GCE. For comparison, GO/GCE, CeO<sub>2</sub>/GCE and ERGO/GCE were also fabricated in a similar way. The brief fabrication process of the CeO<sub>2</sub>/ERGO/GCE and its use in vanillin sensing is shown in Scheme 1.



**Scheme 1.** Synthesis of the sensing material and the construction processes of the proposed CeO<sub>2</sub>/ERGO/GCE for vanillin sensing.

## 2.6. Electrochemical Measurement

For electrochemical measurements, 10 mL 0.10 M HCl solution containing a certain concentration of vanillin was added to a 10 mL cell, and a three-electrode system was installed in the test solution. After accumulation at 0.1 V for 120 s, the cyclic voltammograms were recorded from 0.1 V to 1.2 V and the second-order derivative linear sweep voltammograms were recorded from 0.6 V to 1.2 V. After every measurement, the CeO<sub>2</sub>/ERGO/GCE was regenerated by two successive voltammetric sweeps in 0.6–1.2 V in 0.1 M H<sub>2</sub>SO<sub>4</sub> solution. Sample analysis was carried out under the best conditions.

## 3. Results and Discussion

### 3.1. Morphological and Structural Characterizations

The surface morphology of GO nanosheets, CeO<sub>2</sub> nanoparticles, and CeO<sub>2</sub>/ERGO nanocomposites were studied by SEM. As shown in Figure 1A, the GO layer produced a rough, wrinkled and folded surface. The typical morphology of CeO<sub>2</sub> nanoparticles is shown in Figure 1B. Most of CeO<sub>2</sub> nanoparticles were spherical with a particle size distribution of about 20–200 nm. On the contrary, when CeO<sub>2</sub> and ERGO were mixed together (Figure 1C), it was observed that CeO<sub>2</sub> nanoparticles were wrapped inside by gossamer like ERGO, indicating that CeO<sub>2</sub> and ERGO are well combined. The combination of CeO<sub>2</sub> and ERGO provides a rich conductive channel for the electron transfer of Trp on the electrode surface. The XRD pattern of CeO<sub>2</sub> is shown in Figure 1D. The diffraction peaks located at  $2\theta = 28.6^\circ, 33.0^\circ, 47.3^\circ, 56.2^\circ$  and  $59.2^\circ$  can be easily indexed to (111), (200), (220), (311), and (222) crystal planes of cubic fluorite structure of CeO<sub>2</sub> [JCPDS 34-0394] [37].

The morphology of the as-prepared CeO<sub>2</sub>/ERGO nanocomposite was further examined by TEM. Figure 2A showed the TEM micrograph of the composite. It can be seen that most CeO<sub>2</sub> nanoparticles were well wrapped in the ERGO sheets, and no free CeO<sub>2</sub> nanoparticles were observed outside of the ERGO sheets, indicating a good interfacial interaction between the CeO<sub>2</sub> nanoparticles and the ERGO sheets. The element composition and distribution of CeO<sub>2</sub>-ERGO nanocomposite were analyzed by EDS. As shown in Figure 2B–D, C, O, and Ce elements were observed in the element mapping images of the CeO<sub>2</sub>/ERGO composite. It was worth noting that the three elements were uniformly distributed throughout the CeO<sub>2</sub>/ERGO composite, indicating that the electrochemical reduction method is efficient to synthesize the CeO<sub>2</sub>/ERGO nanocomposite.



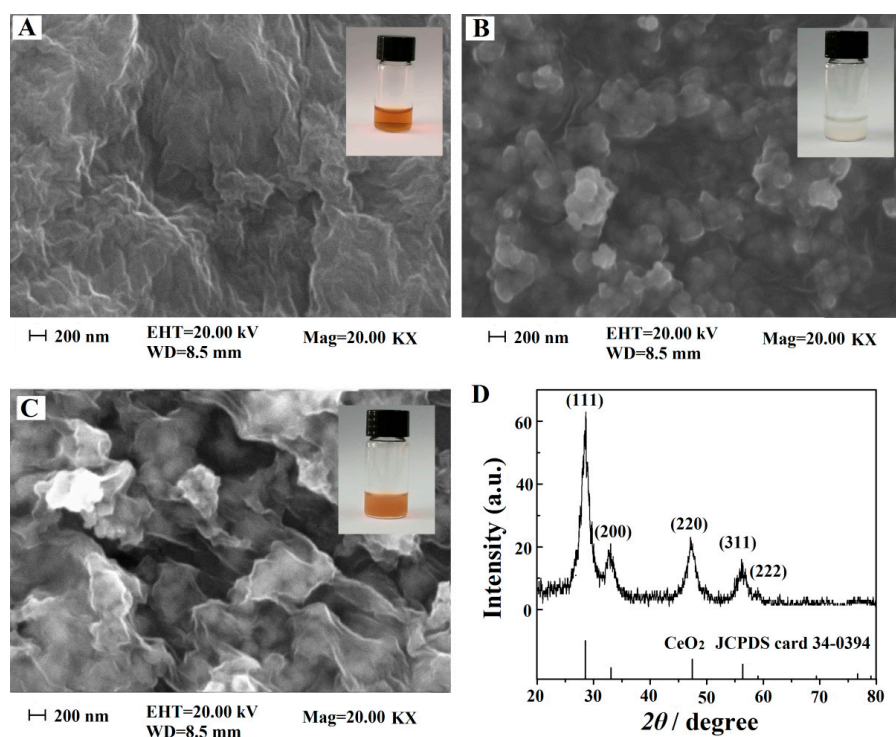


**Figure 1.** SEM images of (A) GO, (B) CeO<sub>2</sub>, (C) CeO<sub>2</sub>/ERGO nanocomposite and (D) the XRD pattern of CeO<sub>2</sub>. Inset: digital camera images of the pure GO, CeO<sub>2</sub> and CeO<sub>2</sub>/ERGO nanocomposite.

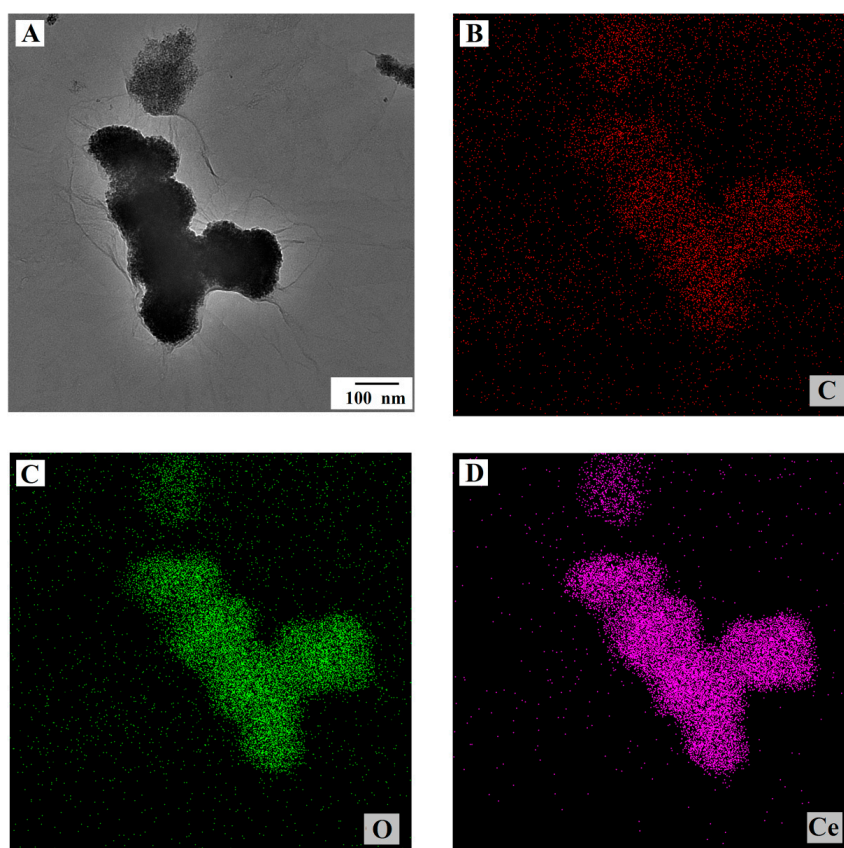


**Figure 2.** (A) TEM image of CeO<sub>2</sub>-ERGO nanocomposite; (B–D) Element mapping images of C, O and Ce of CeO<sub>2</sub>-ERGO composites.

### 3.2. Electrochemical Characterization of the Modified Electrodes

Using 1.0 mM  $K_3[Fe(CN)_6]$  as a probe, The properties of the surface of different electrodes were characterized by CV. Figure 3 exhibited the CV results obtained on bare GCE (a), GO/GCE (b),  $CeO_2$ /GCE (c), and  $CeO_2$ /ERGO/GCE (d) in the potential range of  $-0.2\sim 0.6$  V. On bare GCE a pair of well-defined redox peaks was observed with the peak-to-peak potential separation ( $\Delta E_p$ ) of 85 mV and the redox peak current of  $14.80 \mu A$  ( $I_{pa}$ ) and  $15.87 \mu A$  ( $I_{pc}$ ) (curve a). It was shown that the electron transfer process is quasi-reversible. However, the redox peak current decreased obviously on GO/GCE ( $I_{pa} = 3.994 \mu A$ ,  $I_{pc} = 4.016 \mu A$ ),  $\Delta E_p$  was 167 mV (curve b). This may be due to the poor conductivity of GO and the strong negative charge repulsion force between  $[Fe(CN)_6]^{3-/4-}$  and the ionized groups such as  $COO^-$  in GO. On the other hand, the current response of  $[Fe(CN)_6]^{3-/4-}$  on the  $CeO_2$ /GCE (curve c) increased slightly compared with that of bare GCE. On  $CeO_2$ /ERGO/GCE (curve d), the  $\Delta E_p$  value decreased to 78 mV and the highest redox peak current was observed, suggesting a more reversible electron transfer process of  $[Fe(CN)_6]^{3-/4-}$  occurred on  $CeO_2$ /ERGO/GCE. Therefore, the electron transfer rate was greatly improved due to the coexistence of ERGO and  $CeO_2$  nanoparticles.

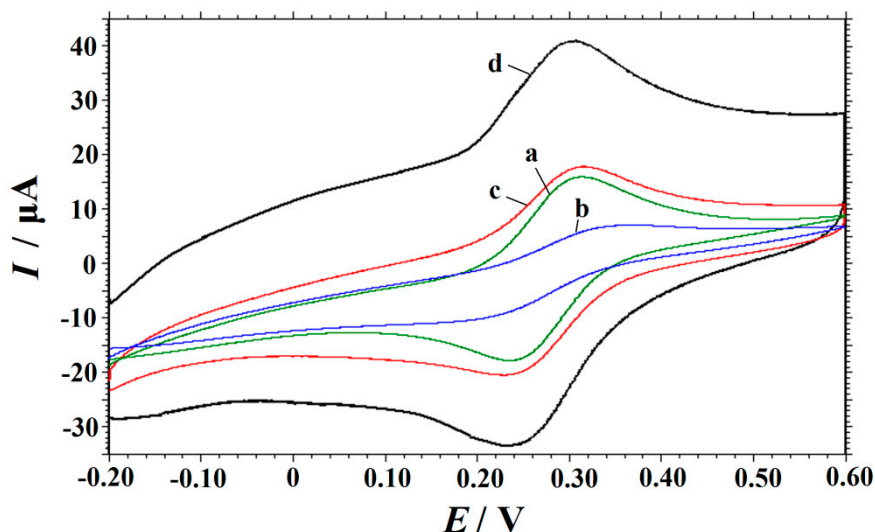


**Figure 3.** CVs of 1.0 mM  $K_3[Fe(CN)_6]$  in 0.5 M KCl recorded at (a) GCE, (b) GO/GCE, (c)  $CeO_2$ /GCE and (d)  $CeO_2$ /ERGO/GCE at a scan rate of  $0.1 \text{ V s}^{-1}$ .

### 3.3. Electrochemical Oxidation of Vanillin at Different Electrodes

The catalytic properties of  $CeO_2$ /ERGO/GCE for vanillin oxidation are confirmed in Figure 4, which showed the CV responses of  $10 \mu M$  vanillin recorded at different electrodes in 0.1 M HCl solution. On the  $CeO_2$ /ERGO/GCE, a well-defined and sensitive vanillin oxidation peak ( $P_1$ ) appeared at 0.942 V [12,13]. In addition to the oxidation peak at 0.942 V, a redox couple  $P_2/P_3$  ( $E_{pa} = 0.688 \text{ V}$ ,  $E_{pc} = 0.630 \text{ V}$ ) was also observed, corresponding to the redox reaction of the oxidized intermediate of vanillin. The electrochemical reaction mechanism was illustrated in Scheme 2 [12,13]. Table 1 compared the electrochemical data of vanillin obtained on different electrodes. It can be clearly observed that an obvious oxidation peak ( $I_p = 25.24 \mu A$ ) appeared at 0.949 V at the ERGO/GCE compared with other electrodes, which may be related to the good catalytic activity, high conductivity, and large surface area of ERGO. The maximum oxidation peak current was obtained at  $CeO_2$ /ERGO/GCE, which is about two times higher than that of ERGO/GCE, demonstrating the synergistic effect of  $CeO_2$  nanoparticles and ERGO nanosheets were existed on the electrode surface. As shown in Table 1, the order of the ability to enhance the oxidation signals of vanillin is  $CeO_2$ /ERGO/GCE > ERGO/GCE >  $CeO_2$ /GO/GCE > GO/GCE >  $CeO_2$ /GCE > bare GCE. In particular, ERGO nanosheets have excellent conductivity and high surface area. Also the electron exchange between  $CeO_2$  nanoparticles and vanillin promoted the electrocatalytic reaction. In addition, ERGO is a good supporter for  $CeO_2$  nanoparticles, which can

effectively prevent the agglomeration of CeO<sub>2</sub> nanoparticles and give full play to its catalytic property. Therefore, the interface conductivity of the modified electrode was greatly improved and the sensitivity of the determination of vanillin was improved.

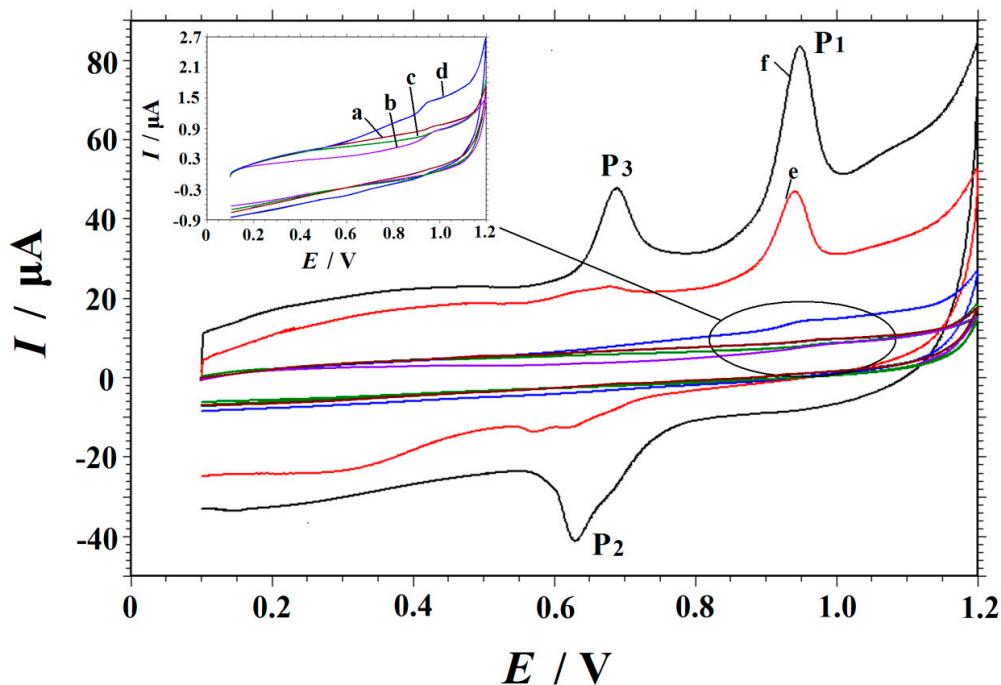
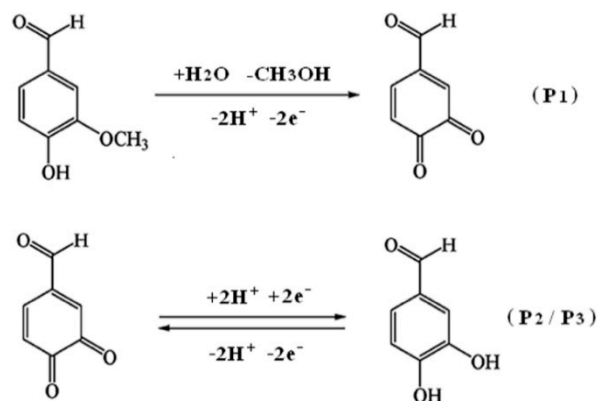


**Figure 4.** CVs obtained on different electrodes in 0.1 M HCl solution containing 10  $\mu\text{M}$  vanillin (a: bare GCE; b: GO/GCE; c: CeO<sub>2</sub>/GCE; d: CeO<sub>2</sub>/GO/GCE; e: ERGO/GCE; f: CeO<sub>2</sub>/ERGO/GCE). Scan rate: 0.1 V·s<sup>-1</sup>.



**Scheme 2.** Oxidation mechanism of vanillin on the CeO<sub>2</sub>/ERGO/GCE.

**Table 1.** Detailed data of CVs of 10  $\mu\text{M}$  vanillin recorded at different electrodes.

Electrode	$I_p/\mu\text{A}$	$E_p/\text{V}$
GCE	0.3242	0.978
GO/GCE	0.6226	0.979
CeO <sub>2</sub> /GCE	0.3469	0.980
CeO <sub>2</sub> /GO/GCE	1.146	0.953
ERGO/GCE	25.24	0.949
CeO <sub>2</sub> /ERGO/GCE	52.22	0.942

### 3.4. Effect of Scan Rate

In order to further investigate the oxidation mechanism, the CVs of 10  $\mu\text{M}$  vanillin recorded on the  $\text{CeO}_2/\text{ERGO}/\text{GCE}$  under different scan rates were illustrated in Figure 5A. Obviously, the oxidation peak increased gradually with the increase of scan rate in the range of 0.03–0.3  $\text{V s}^{-1}$ . A good linear relationship between the peak current ( $I_p$ ) and scan rate ( $\nu$ ) was observed in Figure 5B. The corresponding regression equation was  $I_p (\mu\text{A}) = 0.1929 \nu (\text{V s}^{-1}) - 0.4991$  ( $R = 0.9959$ ). It shows that the oxidation process of vanillin on the  $\text{CeO}_2/\text{ERGO}/\text{GCE}$  is controlled by adsorption. By plotting the relationship between logarithm  $I_p$  and logarithm  $\nu$ , the adsorption control behavior of vanillin was further confirmed:  $\log I_p (\mu\text{A}) = 1.0371 \log \nu (\text{V s}^{-1}) + 2.3049$  ( $R = 0.9987$ ). The obtained slope of 1.0371 is close to 1.0. In Figure 5C, it is worth noting that the  $E_p$  of vanillin moved to a positive value with the increase of scan rate, and  $E_p$  changed linearly versus Napierian logarithm of scan rate ( $\ln \nu$ ). The linear regression equation was  $E_p (\text{V}) = 0.0214 \ln \nu (\text{V s}^{-1}) + 0.9966$  ( $R = 0.9981$ ). For a completely irreversible adsorption control process,  $E_p$  can be expressed by the Laviron equation [43]:

$$E_p = E^{0'} + (RT/\alpha nF) \ln (RTk^0/\alpha nF) + (RT/\alpha nF) \ln \nu \quad (1)$$

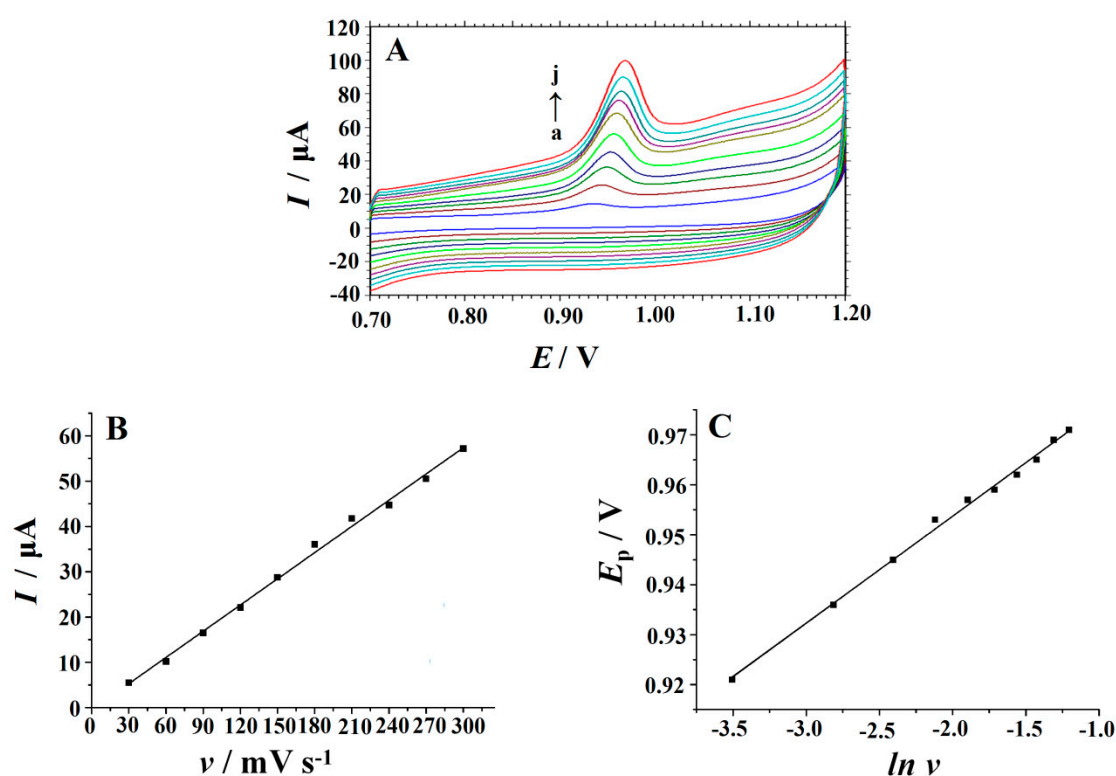


**Figure 5.** (A) CVs recorded at the  $\text{CeO}_2/\text{ERGO}/\text{GCE}$  in 10  $\mu\text{M}$  vanillin solution at different scan rates (a–j: 0.03, 0.06, 0.09, 0.12, 0.15, 0.18, 0.21, 0.24, 0.27, 0.30  $\text{V s}^{-1}$ ); (B) The dependence of peak current on scan rate ( $\nu$ ); (C) The dependence of peak potential on  $\ln \nu$ .

According to equation (1), the slope of the straight line is equal to  $RT/\alpha nF$ , so  $\alpha n$  was calculated as 1.196.  $\alpha$  is approximately 0.5 in a completely irreversible electrode process, thus  $n$  is about 2, which is consistent with the results obtained on silver nanoplate/GR composite modified GCE [12] and graphene-polyvinylpyrrolidone modified acetylene black paste electrode [13].

### 3.5. Chronocoulometric Studies

Using chronocoulometry, the diffusion coefficient  $D$  and Faradic charge  $Q_{\text{ads}}$  of vanillin at the  $\text{CeO}_2/\text{ERGO}/\text{GCE}$  were calculated. Figure 6A showed the plot of  $Q-t$  obtained in the 0.1 M HCl



solution with and without 0.1 mM vanillin. After background subtraction and the plot of charge ( $Q$ ) against the square root of time ( $t^{1/2}$ ) (Figure 6B), a good linear relationship was observed with a slope of  $1.729 \times 10^{-5} \text{ C s}^{-1/2}$  and  $Q_{\text{ads}}$  of  $1.679 \times 10^{-5} \text{ C}$ . Using Equation (2) given by Anson [44],  $D$  can be obtained:

$$Q = 2nFACD^{1/2} \pi^{-1/2} t^{1/2} + Q_{dl} + Q_{\text{ads}} \quad (2)$$

where  $Q_{dl}$  is double layer charge,  $A$  is the electrode surface area, and  $c$  is the substrate concentration. According to Figure 3, using Randles–Sevcik Equation (3) [45],  $A$  was estimated to be  $0.01478 \text{ cm}^2$ .

$$I_p = 2.69 \times 10^5 n^{3/2} A_{\text{eff}} D^{1/2} \nu^{1/2} C \quad (3)$$

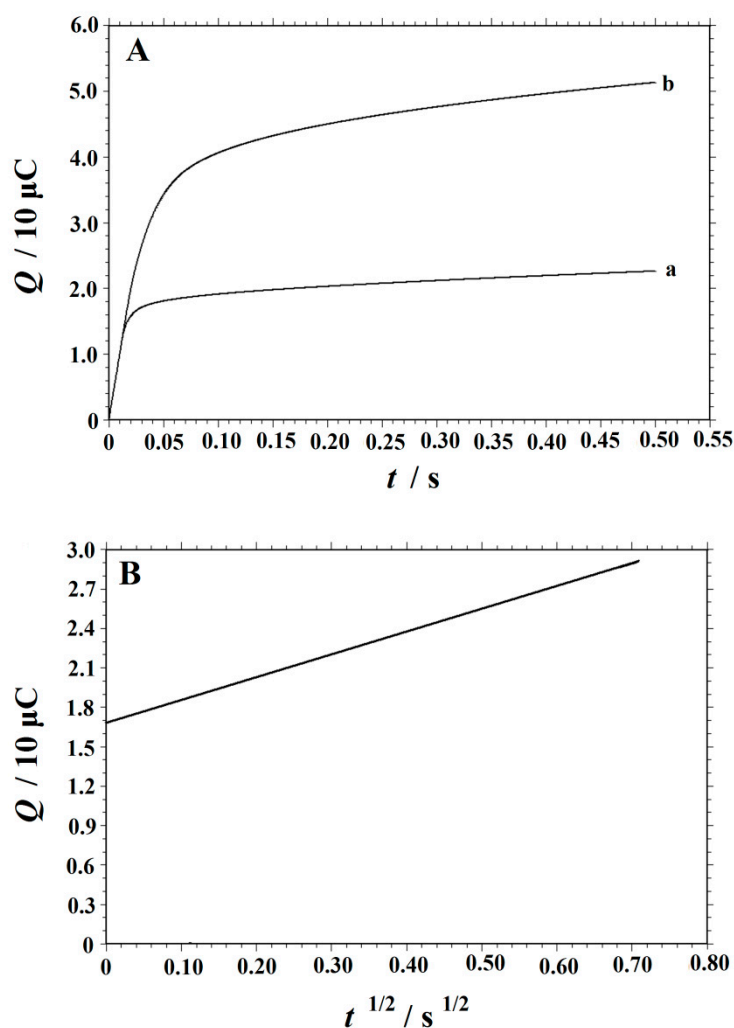


**Figure 6.** (A) Plot of  $Q-t$  curve obtained on the  $\text{CeO}_2/\text{ERGO}/\text{GCE}$  in 0.1 M HCl solution in the absence (a) and presence (b) of 0.1 mM vanillin. (B) plot of  $Q-t^{1/2}$  curve on the  $\text{CeO}_2/\text{ERGO}/\text{GCE}$  (background subtracted).

Thus,  $D$  of  $2.9 \times 10^{-5} \text{ cm}^2 \text{ s}^{-1}$  was obtained. According to the equation  $Q_{\text{ads}} = nFA \Gamma_s$ , the adsorption capacity  $\Gamma_s$  was obtained as  $5.88 \times 10^{-10} \text{ mol cm}^{-2}$ .

For the completely irreversible oxidation of vanillin at the  $\text{CeO}_2/\text{ERGO}/\text{GCE}$ , the standard heterogeneous rate constant ( $k_s$ ) can be obtained based on Equation (4) [46,47]:

$$k_s = 2.415 \exp(-0.02F/RT) D^{1/2} (E_p - E_{p/2})^{-1/2} \nu^{1/2} \quad (4)$$

In the formula,  $E_p$  represents the peak potential,  $E_{p/2}$  is the potential at which  $I = I_p/2$ . Other symbols have their usual meanings. In our experiment,  $E_p - E_{p/2} = 34$  mV,  $D = 2.9 \times 10^{-5}$  cm<sup>2</sup> s<sup>-1</sup>,  $v = 100$  mV s<sup>-1</sup>, and  $T = 298$  K. The value of  $k_s$  was obtained as  $1.02 \times 10^{-2}$  cm s<sup>-1</sup>, confirming a relative rapid electrode reaction process.

### 3.6. Optimal of Some Determination Conditions

The electrochemical response of vanillin on the CeO<sub>2</sub>/ERGO/GCE was investigated in different types of supporting electrolytes, such as HAc–NH<sub>4</sub>Ac buffer solution (pH 4.0), phosphate buffer solution (pH 3.0 and 6.0), HAc–NaAc buffer solution (pH 4.0), HCl, H<sub>2</sub>SO<sub>4</sub>, HNO<sub>3</sub>, and H<sub>3</sub>PO<sub>4</sub> (each 0.1 M). It was found that the peak current was the largest and the peak shape was sharp in HCl solution. In the range of 0.02–0.5 M, the effect of HCl concentration on the peak current of 10 μM vanillin was studied. It was found that the maximum peak current of vanillin was obtained when the concentration of HCl reached 0.1–0.2 M (Figure 7). In this experiment, 0.1 M HCl solution was selected for vanillin detection.

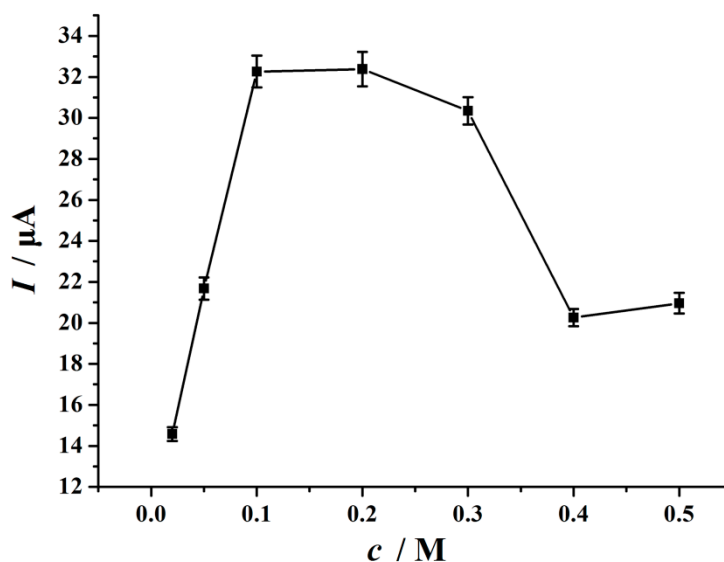


**Figure 7.** Effect of HCl concentration on the peak current of 10 μM vanillin at CeO<sub>2</sub>/ERGO/GCE.

Since the electrode process of vanillin on the CeO<sub>2</sub>/ERGO/GCE is controlled by adsorption, the accumulation conditions have a great influence on the peak current of vanillin. As showed in Figure 8A, when the accumulation potential changed in the range of  $-0.3$ – $0.3$  V, the peak current of vanillin increased first and then decreased, and reached the maximum value at 0.1 V. As shown in in Figure 8B, the peak current was greatly affected by the accumulation time. In the initial 120 s, the peak current increased significantly, and then the peak current tended to be stable when the time exceeded 120 s. This may be due to the saturated adsorption of vanillin. Therefore, the accumulation conditions (0.1 V, 120 s) were selected for vanillin detection.

### 3.7. Linear Range and Detection Limit

Compared with the traditional CV method, the second-order derivative linear sweep voltammetry (SDLSV) has the advantages of low detection limit and high sensitivity, and is a more effective electrochemical technique for quantitative analysis. Therefore, SDLSV was used for the determination of vanillin in this study. Figure 9A,B showed the voltammetric curves of vanillin at different concentrations on the CeO<sub>2</sub>/ERGO/GCE under the optimized conditions. The proportional of well-defined peak current to vanillin concentration was observed in Figure 9C,D and the calibration curve in the form of  $I_p$  versus concentration of vanillin showed two linear regions from 0.04 to 20 μM and 20–100 μM with the

equations of  $I (\mu\text{A}) = 3.003c (\mu\text{M}) + 0.7587$  ( $R = 0.9941$ ) and  $I (\mu\text{A}) = 0.4582c (\mu\text{M}) + 48.159$  ( $R = 0.9836$ ), respectively. The detection limit was  $0.01 \mu\text{M}$ . In order to estimate the analytical characteristics of the developed sensor, the  $\text{CeO}_2/\text{ERGO}/\text{GCE}$  was comprehensively compared with other published electrochemical methods for vanillin detection. From the results in Table 2, it was found that, compared with other electrodes, the developed  $\text{CeO}_2/\text{ERGO}/\text{GCE}$  has better detection performance with a wider dynamic range and lower detection limit.

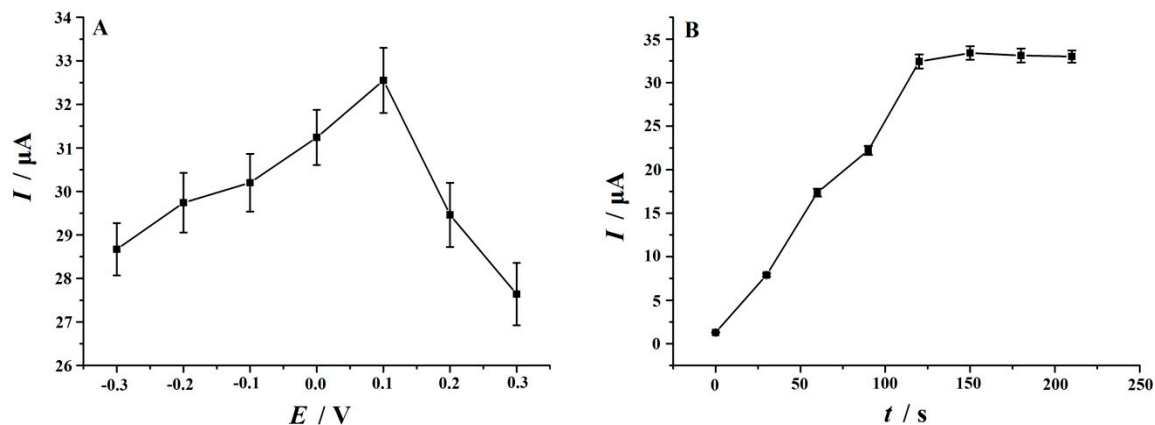


**Figure 8.** (A) The effect of accumulation potential (A) and accumulation time (B) on the peak current. Vanillin concentration:  $10 \mu\text{M}$ , supporting electrolyte:  $0.1 \text{ M HCl}$ , scan rate:  $0.1 \text{ V s}^{-1}$ .

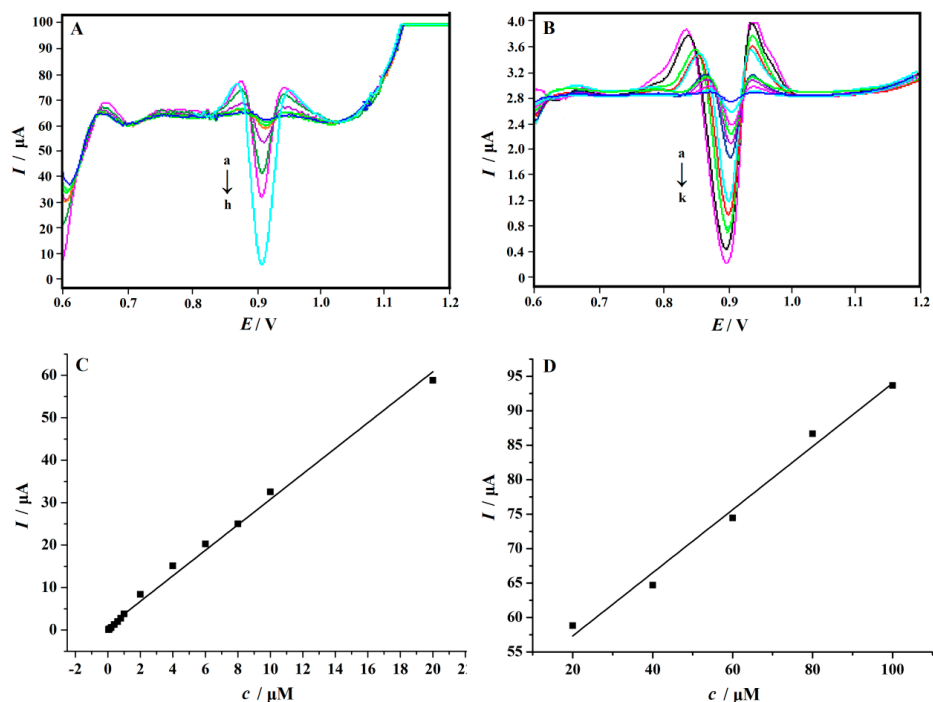


**Figure 9.** SDLSVs of different concentration of vanillin in  $0.1 \text{ M HCl}$  solution recorded at the  $\text{CeO}_2/\text{ERGO}/\text{GCE}$  after accumulation at  $0.1 \text{ V}$  for  $120 \text{ s}$  at a scan rate of  $0.1 \text{ V s}^{-1}$ . (A) a-h:  $0.04, 0.06, 0.08, 0.1, 0.2, 0.4, 0.6, 0.8 \mu\text{M}$ ; (B) a-k:  $1, 2, 4, 6, 8, 10, 20, 40, 60, 80, 100 \mu\text{M}$ . (C) Calibration curve ( $C_{\text{vanillin}} = 0.04\text{--}20 \mu\text{M}$ ) and (D) Calibration curve ( $C_{\text{vanillin}} = 20\text{--}100 \mu\text{M}$ ).

**Table 2.** Comparison of properties of different modified electrodes for the detection of vanillin.

Electrochemical Sensors	Technique	Linear Range / $\mu\text{M}$	Detection Limit / $\mu\text{M}$	References
<sup>a</sup> AuPd-GR/GCE	<sup>k</sup> DPV	0.1–7; 10–40	0.02	[9]
<sup>b</sup> CoS NR@Nafion/GCE	DPV	0.5–56	0.07	[10]
<sup>c</sup> MoS <sub>2</sub> -CNF/GCE	amperometry	0.3–135	0.15	[11]
<sup>d</sup> Ag NPs/GN/GCE	<sup>l</sup> SWV	2–100	0.332	[12]
<sup>e</sup> GR-PVP/ABPE	SDLSV	0.02–2.0; 2.0–40; 40–100	0.01	[13]
<sup>f</sup> BDD electrode	<sup>m</sup> SWASV	3.3–330	0.38	[14]
<sup>g</sup> APT-BDD	SWASV	6.6–660	1.47	[15]
<sup>h</sup> CTABMGPE	DPV	4–15; 20–70	1.29	[16]
<sup>i</sup> Ag-Pd/GO/GCE	DPV	0.02–45	0.005	[17]
<sup>j</sup> MWNTs-PDA@ MIP/SWNTsCOOH/GCE	DPV	0.2–10	0.1	[18]
CeO <sub>2</sub> -ERGO/GCE	SDLSV	0.04–20; 20–100	0.01	This work

<sup>a</sup> Au-Pd nanoparticles-graphene/GCE; <sup>b</sup> CoS nanorods (NR) @Nafion/GCE; <sup>c</sup> electrospun molybdenum disulfide/carbon nanofibers/GCE; <sup>d</sup> silver nanoplates/grapheme/GCE; <sup>e</sup> graphene-polyvinylpyrrolidone/GCE; <sup>f</sup> cathodically pretreated boron-doped diamond electrode; <sup>g</sup> anodically pretreated boron-doped diamond electrode; <sup>h</sup> ionic surfactant modified graphene paste electrode; <sup>i</sup> Ag-Pd bimetallic nanoparticles/graphene oxide/GCE; <sup>j</sup> molecularly imprinted poly(1-vinyl-3-octylimidazole hexafluoride phosphorus)-multi-walled carbon nanotubes@polydopamine-carboxyl single-walled carbon nanotubes composite/GCE; <sup>k</sup> differential pulse voltammetry; <sup>l</sup> square-wave voltammetry; <sup>m</sup> square-wave adsorptive stripping voltammetry.

### 3.8. Reproducibility, Stability and Selectivity of CeO<sub>2</sub>/ERGO/GCE

Seven CeO<sub>2</sub>/ERGO/GCEs were fabricated by the same method to test the reproducibility, and 10  $\mu\text{M}$  vanillin solution was measured under the same conditions. The relative standard deviation (RSD) of 4.62% ( $n = 7$ ) indicated excellent reproducibility. In addition, to test the repeatability, the vanillin solution was determined by a single CeO<sub>2</sub>/ERGO/GCE for 10 times. After each measurement, to regenerate the electrode surface, two successive voltammetric sweeps were carried out in 0.1 M H<sub>2</sub>SO<sub>4</sub> solution in the range of 0.2–1.2 V. The good repeatability was reflected by the RSD of 2.74%. The storage stability of the modified electrode was also evaluated by storing the modified electrode in air. After two weeks, the response of the electrode is still 91.6% of the initial current, which showed that the electrode has long-term stability. In addition, it was found that when a 1000-fold amount of sucrose, glucose, fructose, K<sup>+</sup>, Ca<sup>2+</sup>, Na<sup>+</sup>, Mg<sup>2+</sup>, Zn<sup>2+</sup>, Al<sup>3+</sup>, and a 500-fold amount of citric acid, tartaric acid, lactic acid, and caffeine were present, the peak current change of 10  $\mu\text{M}$  vanillin was less than 5%. Ascorbic acid (AA), uric acid (UA) and dopamine (DA) as three kinds of important biological substances in the human fluid. Figure 10 exhibited the SDLSVs obtained at the CeO<sub>2</sub>/ERGO/GCE in the presence of 1.0 mM AA, 10  $\mu\text{M}$  DA, 10  $\mu\text{M}$  UA, and 1.0  $\mu\text{M}$  vanillin. As shown in Figure 10, four oxidation peaks were well separated in 0.1 M HCl solution, the oxidation peak potentials of AA, DA, UA and vanillin were 0.248 V, 0.473 V, 0.620 V, and 0.918 V, respectively. It was found that there was no obvious interference for the oxidation signal of vanillin (signal change below  $\pm 5\%$ ).

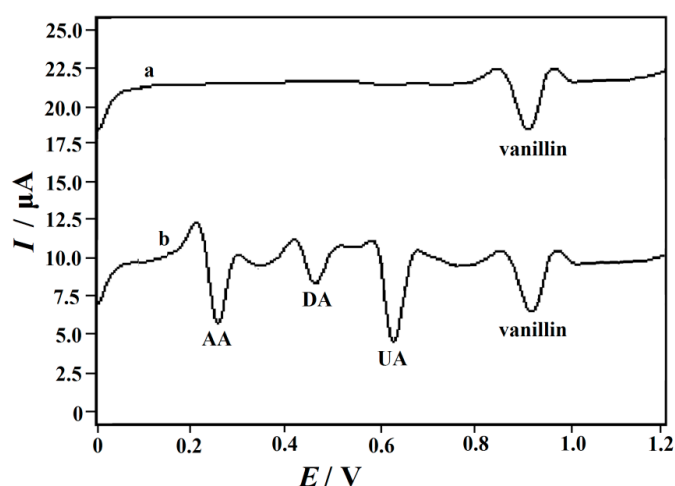


**Figure 10.** SDLSVs obtained at the CeO<sub>2</sub>/ERGO/GCE in 0.1 M HCl solution containing (a) 1.0 μM vanillin; (b) 1.0 mM AA+ 10 μM DA + 10 μM UA + 1.0 μM vanillin. Accumulation potential: 0.1 V, accumulation time: 120 s, scan rate: 0.1 V s<sup>-1</sup>.

### 3.9. Application

The determination of vanillin in commercial food products such as biscuit, chocolate and pudding powder was performed using the developed method. The sample solutions were prepared according to reference [13], and the results were listed in Table 3. The contents of vanillin in these samples were calculated as 46.25 μg g<sup>-1</sup> (for biscuit), 69.38 μg g<sup>-1</sup> (for chocolate) and 132.98 μg g<sup>-1</sup> (for pudding powder), respectively. The recoveries were 97.0–104.0%, which showed that the method can be used for the accurate and rapid detection of vanillin in commercial food samples.

**Table 3.** Determination results of vanillin in food samples.

Samples	Added/μM	Found/μM	RSD/%	Recovery/%
Biscuit	0	1.52	2.86	-
	1.0	2.56	3.19	104.0
	2.0	3.48	2.14	98.0
Chocolate	0	2.28	2.37	-
	1.0	3.25	2.75	97.0
	2.0	4.32	2.84	102.0
Pudding powder	0	4.37	2.16	-
	2.0	6.44	2.51	103.5
	4.0	8.30	2.83	98.3

## 4. Conclusions

In this paper, CeO<sub>2</sub> nanoparticles were synthesized by the hydrothermal method and dispersed uniformly in graphene oxide (GO) aqueous solution by ultrasonication. The homogeneous CeO<sub>2</sub>-GO dispersion was coated on the surface of a glassy carbon electrode (GCE), and GO was converted into ERGO by potentiostatic reduction to obtain the modified electrode (CeO<sub>2</sub>/ERGO/GCE). This method offers several advantages over other techniques, including being green, efficient, inexpensive, and rapid. The electrochemical behaviors of vanillin on the CeO<sub>2</sub>/ERGO/GCE were studied carefully and the electrochemical parameters were calculated. The obtained CeO<sub>2</sub>/ERGO nanocomposite exhibited excellent performance for vanillin oxidation due to its strong electrocatalytic ability, good conductivity, and large surface area. Using the SDLSV technique, vanillin can be detected in the concentration range of 0.04–20 μM and 20–100 μM with the detection limit of 0.01 μM. Furthermore, the developed method



has the advantages of high sensitivity, good selectivity, simple electrode preparation, and low cost. It has a wide application prospect in the sensitive detection of vanillin in commercial foods.

**Author Contributions:** Y.T., H.W., X.N., and P.D. conceived and designed the experimental works; X.N. performed the experimental works and worked on data analyses; R.Z. and Z.T. contributed materials, reagents and analysis tools used in this study; Y.T. and X.N. drafted the first version of the manuscript. All authors have read and agreed to the published version of the manuscript.

**Funding:** This research was financially supported by the National Nature Science Foundation of China (No. 21571189, No. 21671200, No. U19A2019 and No. 21975289), the Opening Projects of Key Laboratory of Functional Organometallic Materials, University of Hunan Province (GN20K04, GN19K05).

**Conflicts of Interest:** The authors declare no conflict of interest.

## References

1. Millour, S.; Noel, L.; Kadar, A.; Chekri, R.; Vastel, C.; Sirot, B.; Leblanc, J.; Guerin, T. Pb, Hg, Cd, As, Sb and Al levels in foodstuffs from the 2nd French total diet study. *Food Chem.* **2011**, *126*, 1787. [[CrossRef](#)] [[PubMed](#)]
2. Yardım, Y.; Gülcan, M.; Şentürk, Z. Determination of vanillin in commercial food product by adsorptive stripping voltammetry using a boron-doped diamond electrode. *Food Chem.* **2013**, *141*, 1821–1827. [[CrossRef](#)]
3. Pérez-Silva, A.; Odoux, E.; Brat, P.; Ribeyre, F.; Rodriguez-Jimenes, G.; Robles-Olvera, V.; García-Alvarado, M.A.; Günata, Z. GC–MS and GC–olfactometry analysis of aroma compounds in a representative organic aroma extract from cured vanilla (*Vanilla planifolia* G. Jackson) beans. *Food Chem.* **2006**, *99*, 728–735.
4. Pérez-Esteve, É.; Lerma-García, M.J.; Fuentes, A.; Palomares, C.; Barat, J.M. Control of undeclared flavoring of cocoa powders by the determination of vanillin and ethyl vanillin by HPLC. *Food Control* **2016**, *67*, 171–176. [[CrossRef](#)]
5. Gerasimov, A.V.; Gornova, N.V.; Rudometova, N.V. Determination of vanillin and ethylvanillin in vanilla flavorings by planar (thin-layer) chromatography. *J. Anal. Chem.* **2003**, *58*, 677–684. [[CrossRef](#)]
6. Altunay, N. Development of vortex-assisted ionic liquid-dispersive microextraction methodology for vanillin monitoring in food products using ultraviolet-visible spectrophotometry. *LWT* **2018**, *93*, 9–15. [[CrossRef](#)]
7. Timotheou-Potamia, M.; Calokerinos, A.C. Chemiluminometric determination of vanillin in commercial vanillin products. *Talanta* **2007**, *71*, 208–212. [[CrossRef](#)]
8. Minematsu, S.; Xuan, G.S.; Wu, X.Z. Determination of vanillin in vanilla perfumes and air by capillary electrophoresis. *J. Environ. Sci.* **2013**, *25*, s8–s14. [[CrossRef](#)]
9. Shang, L.; Zhao, F.; Zeng, B. Sensitive voltammetric determination of vanillin with an AuPd nanoparticles graphene composite modified electrode. *Food Chem.* **2014**, *151*, 53–57. [[CrossRef](#)]
10. Sivakumar, M.; Sakthivel, M.; Chen, S.M. Simple synthesis of cobalt sulfide nanorods for efficient electrocatalytic oxidation of vanillin in food samples. *J. Colloid Interface Sci.* **2017**, *490*, 719–726. [[CrossRef](#)]
11. Mei, Q.; Ding, Y.; Li, L.; Wang, A.; Zhao, Y. Electrospun MoS<sub>2</sub> composite carbon nanofibers for determination of vanillin. *J. Electroanal. Chem.* **2019**, *833*, 297–303.
12. Huang, L.; Hou, K.; Jia, X.; Pan, H.; Du, M. Preparation of novel silver nanoplates/graphene composite and their application in vanillin electrochemical detection. *Mater. Sci. Eng. C* **2014**, *38*, 39–45. [[CrossRef](#)] [[PubMed](#)]
13. Deng, P.; Xu, Z.; Zeng, R.; Ding, C. Electrochemical behavior and voltammetric determination of vanillin based on an acetylene black paste electrode modified with graphene–polyvinylpyrrolidone composite film. *Food Chem.* **2015**, *180*, 156–163. [[CrossRef](#)] [[PubMed](#)]
14. Alpar, N.; Yardım, Y.; Şentürk, Z. Selective and simultaneous determination of total chlorogenic acids, vanillin and caffeine in foods and beverages by adsorptive stripping voltammetry using a cathodically pretreated boron-doped diamond electrode. *Sens. Actuators B Chem.* **2018**, *257*, 398–408. [[CrossRef](#)]
15. Ali, H.S.; Abdullah, A.A.; Pinar, P.T.; Yardım, Y.; Şentürk, Z. Simultaneous voltammetric determination of vanillin and caffeine in food products using an anodically pretreated boron-doped diamond electrode: Its comparison with HPLC-DAD. *Talanta* **2017**, *170*, 384–391. [[CrossRef](#)]
16. Raril, C.; Manjunatha, J.G. A simple approach for the electrochemical determination of vanillin at ionic surfactant modified graphene paste electrode. *Microchem. J.* **2020**, *154*, 104575. [[CrossRef](#)]

17. Li, J.; Feng, H.; Li, J.; Jiang, J.; Feng, Y.; He, L.; Qian, D. Bimetallic Ag-Pd nanoparticles-decorated graphene oxide: A fascinating three-dimensional nano-hybrid as an efficient electrochemical sensing platform for vanillin determination. *Electrochim. Acta* **2015**, *176*, 827–835. [[CrossRef](#)]
18. Wu, W.; Yang, L.; Zhao, F.; Zeng, B. A vanillin electrochemical sensor based on molecularly imprinted poly(1-vinyl-3-octylimidazole hexafluoride phosphorus)-multi-walled carbon nanotubes@polydopamine-carboxyl single-walled carbon nanotubes composite. *Sens. Actuators B Chem.* **2017**, *239*, 481–487. [[CrossRef](#)]
19. He, Q.; Liu, J.L.X.; Li, G.; Chen, D.; Deng, P.; Liang, J. A promising sensing platform toward dopamine using MnO<sub>2</sub> nanowires/electro-reduced graphene oxide composites. *Electrochim. Acta* **2019**, *296*, 683–692. [[CrossRef](#)]
20. Malik, R.; Tomer, V.K.; Mishra, Y.K.; Lin, L. Functional gas sensing nanomaterials: A panoramic view. *Appl. Phys. Rev.* **2020**, *7*, 021301–021359. [[CrossRef](#)]
21. Deng, P.; Xu, Z.; Li, J. Simultaneous voltammetric determination of 2-nitrophenol and 4-nitrophenol based on an acetylene black paste electrode modified with a graphene-chitosan composite. *Microchim. Acta* **2014**, *181*, 1077–1084. [[CrossRef](#)]
22. Li, J.; Jiang, J.; Xu, Z.; Liu, M.; Tang, S.; Yang, C.; Qian, D. Facile synthesis of Ag@Cu<sub>2</sub>O heterogeneous nanocrystals decorated N-doped reduced graphene oxide with enhanced electrocatalytic activity for ultrasensitive detection of H<sub>2</sub>O<sub>2</sub>. *Sens. Actuators B Chem.* **2018**, *260*, 529–540. [[CrossRef](#)]
23. Li, J.; Jiang, J.; Xu, Z.; Liu, M.; Tang, S.; Yang, C.; Qian, D. Facile synthesis of Pd-Cu@Cu<sub>2</sub>O/N-RGO hybrid and its application for electrochemical detection of tryptophan. *Electrochim. Acta* **2018**, *260*, 526–535. [[CrossRef](#)]
24. He, Q.; Tian, Y.; Wu, Y.; Liu, J.; Li, G.; Deng, P.; Chen, D. Facile and Ultrasensitive Determination of 4-Nitrophenol Based on Acetylene Black Paste and Graphene Hybrid Electrode. *Nanomaterials* **2019**, *9*, 429. [[CrossRef](#)] [[PubMed](#)]
25. Wu, Y.; Deng, P.; Tian, Y.; Magesa, F.; Liu, J.; Li, G.; He, Q. Construction of effective electrochemical sensor for the determination of quinoline yellow based on different morphologies of manganese dioxide functionalized graphene. *J. Food Compos. Anal.* **2019**, *84*, 103280. [[CrossRef](#)]
26. Tian, Y.; Deng, P.; Wu, Y.; Li, J.; Liu, J.; Li, G.; He, Q. MnO<sub>2</sub> Nanowires-Decorated Reduced Graphene Oxide Modified Glassy Carbon Electrode for Sensitive Determination of Bisphenol A. *J. Electrochem. Soc.* **2020**, *167*, 046514. [[CrossRef](#)]
27. Haldorai, Y.; Yeon, S.H.; Huh, Y.S.; Han, Y.K. Electrochemical determination of tryptophan using a glassy carbon electrode modified with flower-like structured nanocomposite consisting of reduced graphene oxide and SnO<sub>2</sub>. *Sens. Actuators B Chem.* **2017**, *239*, 1221–1230. [[CrossRef](#)]
28. He, Q.; Liu, J.; Liu, X.; Li, G.; Chen, D.; Deng, P.; Liang, J. Fabrication of amine-modified magnetite-electrochemically reduced graphene oxide nanocomposite modified glassy carbon electrode for sensitive dopamine determination. *Nanomaterials* **2018**, *8*, 194. [[CrossRef](#)]
29. He, Q.; Wu, Y.; Tian, Y.; Li, G.; Liu, J.; Deng, P.; Chen, D. Facile electrochemical sensor for nanomolar rutin detection based on magnetite nanoparticles and reduced graphene oxide decorated electrode. *Nanomaterials* **2019**, *9*, 115. [[CrossRef](#)]
30. Balla, P.; Sinha, A.; Wu, L.; Lu, X.; Tan, D.; Chen, J. Co<sub>3</sub>O<sub>4</sub> nanoparticles supported mesoporous carbon framework interface for glucose biosensing. *Talanta* **2019**, *203*, 112–121.
31. He, Q.; Tian, Y.; Wu, Y.; Liu, J.; Li, G.; Deng, P.; Chen, D. Electrochemical sensor for rapid and sensitive detection of tryptophan by a Cu<sub>2</sub>O nanoparticles coated reduced graphene oxide nanocomposite. *Biomolecules* **2019**, *9*, 176. [[CrossRef](#)] [[PubMed](#)]
32. He, Q.; Liu, J.; Tian, Y.; Wu, Y.; Magesa, F.; Deng, P.; Li, G. Facile Preparation of Cu<sub>2</sub>O Nanoparticles and Reduced Graphene Oxide Nanocomposite for Electrochemical Sensing of Rhodamine B. *Nanomaterials* **2019**, *9*, 958. [[CrossRef](#)] [[PubMed](#)]
33. He, Q.; Liu, J.; Liu, X.; Li, G.; Deng, P.; Liang, J. Preparation of Cu<sub>2</sub>O-reduced graphene nanocomposite modified electrodes towards ultrasensitive dopamine detection. *Sensors* **2018**, *18*, 199. [[CrossRef](#)]
34. Carbone, M.; Nesticò, A.; Bellucci, N.; Micheli, L.; Palleschi, G. Enhanced performances of sensors based on screen printed electrodes modified with nanosized NiO particles. *Electrochim. Acta* **2017**, *246*, 580–587. [[CrossRef](#)]

35. He, Q.; Liu, J.; Liu, X.; Li, G.; Deng, P.; Liang, J.; Chen, D. Sensitive and selective detection of tartrazine based on TiO<sub>2</sub>-Electrochemically reduced graphene oxide composite-modified electrodes. *Sensors* **2018**, *18*, 1911. [[CrossRef](#)] [[PubMed](#)]
36. Sarpoushi, M.R.; Nasibi, M.; Golozar, M.A.; Shishesaz, M.R.; Borhani, M.R.; Noroozi, S. Electrochemical investigation of graphene/cerium oxide nanoparticles as an electrode material for supercapacitors. *Mater. Sci. Semicond. Process.* **2014**, *26*, 374–378. [[CrossRef](#)]
37. Adarakatti, P.S.; Gangaiah, V.; Siddaramanna, A. Mesoporous CeO<sub>2</sub> nanoparticles modified Glassy carbon electrode for individual and simultaneous determination of Cu(II) and Hg(II): Application to environmental samples. *Mater. Sci. Semicond. Process.* **2018**, *84*, 157–166. [[CrossRef](#)]
38. Cai, M.; Zhu, L.; Ding, Y.; Wang, J.; Li, J.; Du, X. Determination of sulfamethoxazole in foods based on CeO<sub>2</sub>/chitosan nanocomposite-modified electrodes. *Mater. Sci. Eng. C* **2012**, *32*, 2623–2627. [[CrossRef](#)]
39. Dong, J.; Wang, X.; Qiao, F.; Liu, P.; Ai, S. Highly sensitive electrochemical stripping analysis of methyl parathion at MWCNTs–CeO<sub>2</sub>–Au nanocomposite modified electrode. *Sens. Actuators B* **2013**, *186*, 774–780. [[CrossRef](#)]
40. Li, T.; Liu, H. A simple synthesis method of nanocrystals CeO<sub>2</sub> modified rGO composites as electrode materials for supercapacitors with long time cycling stability. *Powder Technol.* **2018**, *327*, 275–281. [[CrossRef](#)]
41. Ojha, G.P.; Pant, B.; Park, S.J.; Park, M.; Kim, H.Y. Synthesis and characterization of reduced graphene oxide decorated with CeO<sub>2</sub>-doped MnO<sub>2</sub> nanorods for supercapacitor applications. *J. Colloid Interface Sci.* **2017**, *494*, 338–344. [[CrossRef](#)]
42. Deng, P.; Xu, Z.; Feng, Y. Acetylene black paste electrode modified with graphene as the voltammetric sensor for selective determination of tryptophan in the presence of high concentrations of tyrosine. *Mater. Sci. Eng. C* **2014**, *35*, 54–60. [[CrossRef](#)] [[PubMed](#)]
43. Laviron, E. Adsorption, autoinhibition and autocatalysis in polarography and in linear potential sweep voltammetry. *J. Electroanal. Chem. Interfacial Electrochem.* **1974**, *52*, 355–393. [[CrossRef](#)]
44. Anson, F.C. Application of potentiostatic current integration to the study of the adsorption of cobalt (III)-(ethylenedinitrilo(tetraacetate) on mercury electrodes. *Anal. Chem.* **1964**, *36*, 932–934. [[CrossRef](#)]
45. Bard, A.J.; Faulkner, L.R. *Electrochemical Methods*, 2nd ed.; Wiley: New York, NY, USA, 2001.
46. Wu, Y.; Deng, P.; Tian, Y.; Ding, Z.; Li, G.; Liu, J.; Zuberi, Z.; He, Q. Rapid recognition and determination of tryptophan by carbon nanotubes and molecularly imprinted polymer-modified glassy carbon electrode. *Bioelectrochemistry* **2020**, *131*, 107393. [[CrossRef](#)]
47. Velasco, J.G. Determination of standard rate constants for electrochemical irreversible processes from linear sweep voltammograms. *Electroanalysis* **1997**, *9*, 880–882. [[CrossRef](#)]

